Spin Superfluidity and Long-Range Transport in Thin-Film Ferromagnets

Hans Skarsvåg,* Cecilia Holmqvist, and Arne Brataas
Department of Physics, Norwegian University of Science and Technology, NO-7491 Trondheim, Norway
(Received 19 June 2015; published 2 December 2015)

In ferromagnets, magnons may condense into a single quantum state. Analogous to superconductors, this quantum state may support transport without dissipation. Recent works suggest that longitudinal spin transport through a thin-film ferromagnet is an example of spin superfluidity. Although intriguing, this tantalizing picture ignores long-range dipole interactions; here, we demonstrate that such interactions dramatically affect spin transport. In single-film ferromagnets, "spin superfluidity" only exists at length scales (a few hundred nanometers in yttrium iron garnet) somewhat larger than the exchange length. Over longer distances, dipolar interactions destroy spin superfluidity. Nevertheless, we predict the reemergence of spin superfluidity in trilayer ferromagnet-normal metal-ferromagnet films that are ~ 1 μm in size. Such systems also exhibit other types of long-range spin transport in samples that are several micrometers in size.

DOI: 10.1103/PhysRevLett.115.237201 PACS numbers: 75.76.+j, 75.70.Ak, 75.78.-n, 85.75.-d

When matter enters a superfluid phase, it behaves similar to a fluid with zero viscosity and can support currents without dissipation. Some ferromagnets have been suggested to exhibit spin superfluidity (SSF) [1–3]. The superfluid spin-drag properties induced by spin transfer and spin pumping (SP) in a normal metal-ferromagnet-normal metal system have recently been computed [4–6]. Related studies have also explored Josephson spin currents between magnon condensates [7]. Experimental studies have suggested that the temporal decrease of magnon condensates is associated with SSF [8].

In the absence of magnetic fields, SSF is indeed an intriguing possibility because its realization would allow spin currents to propagate without significant losses over long distances. These spin transport properties may be useful for low-dissipation interconnects, spin logic devices, and nonvolatile magnetic memory devices. Our work demonstrates that SSF can exist in thin-film ferromagnetic systems, but two ferromagnets (rather than one) are required to cancel long-range dipole interactions. We do not observe signatures of long-range SSF in single-film ferromagnets.

Recent works have hypothesized that easy-plane ferromagnetic thin films exhibit SSF. In this case, the out-of-plane component of the magnetization direction, m_z, is proportional to the SSF density. The canonically conjugate variable is the in-plane angle, ϕ. In the absence of Gilbert damping, the coupled hydrodynamic equations are analogous to the Josephson relations, $\dot{m}_z \sim \nabla^2\phi$ and $\dot{\phi} \sim m_z$. As in a superfluid, the spin waves then exhibit a linear soundlike spectrum [3,4]. The solution to the hydrodynamic equations is a magnetization that performs full 2π rotations with the precession frequency Ω around the z axis and has a small, constant $m_z \propto \Omega$, which depends on the details of the experimental setup. This metastable state carries a spin current, $J_z^s \propto -\nabla\phi$, and has topological properties that protect against dissipation [3]. Spin relaxation induces a finite resistance proportional to the system size [4]. Nevertheless, ferromagnetic insulators (FIs) have exceptionally low spin dissipation rates, and the spin supercurrent decays over a large length scale. Furthermore, the spin-relaxation-induced algebraic decay of the spin supercurrent significantly differs from the exponential decay of the spin current carried by spin waves [9]. Although magnetic anisotropy destroys the linear SSF response, the spin current is predicted to flow with negligible dissipation when the bias is sufficiently large [4,5].

Long-range dipole interactions are known to dramatically affect the spin-wave dispersion in thin films [10,11]. Low-energy magnons strongly interact, and the coupling between them decreases algebraically as they spatially separate. Magnon interactions are equally important for Bose-Einstein condensation [12]. In the previous theoretical investigations of SSF presented in Refs. [1–6], the dipole field was included as an easy-plane anisotropy. However, the dipole interaction also has a dynamical component that was not included in Refs. [1–6]. Considering that it is the long-range nature of this component that qualitatively changes the dispersion of magnons [10], it is natural to expect that dipole interactions also affect the SSF strongly. When the system is smaller than the exchange length, the energy associated with the exchange stiffness dominates, and the system may exhibit SSF. However, the exchange length in FIs, such as yttrium iron garnet (YIG), is ~ 20 nm, and dipole interactions become increasingly important at larger length scales. For SSF to be useful, it must exist over long, hopefully macroscopic, length scales.

In this Letter, we investigate the complete effect of dipole interactions on spin transport through a FI thin film. We consider both square and circular devices (Fig. 1). As expected, dipole interactions completely alter the spin-transport properties. We find that "SSF" can only be

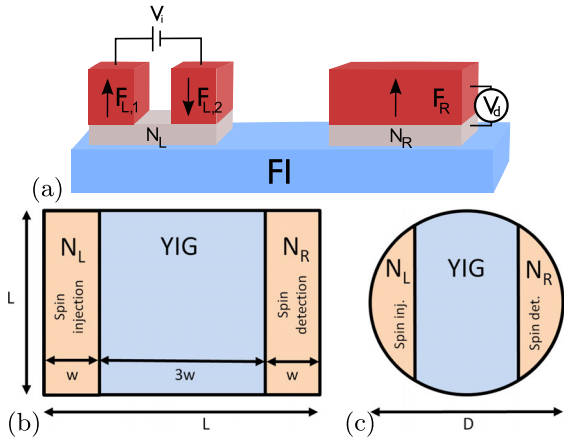

FIG. 1 (color online). (a) A square FI thin film in contact with a spin injector (top left) and a spin detector (top right). A bias voltage V_i injects a spin current via a lateral spin valve in which the ferromagnetic leads have a perpendicular magnetic anisotropy. SP from the FI thin film into the detector induces a voltage V_d. (b) The width of the contacts, w, is 20% of the total length of the FI sample, L. (c) A circular disk with diameter D. The spin injection and detection contacts each cover 20% of the disk area.

achieved when the system size is on the order of the exchange length, which implies that SSF is not a useful method for spin transport across sizable distances. For example, in YIG, which is a widely used FI because of its low dissipation, SSF occurs only across distances of a few hundred nanometers. In comparison, typical spin-wave propagation lengths may reach ~5 mm [13]. Moreover, because of dipole-induced anisotropies, a sufficiently high spin-accumulation bias is required to induce a spin current. As with the spin resistance across the sample, this spin-accumulation threshold strongly depends on the geometry of the system and increases with the system size.

Nonetheless, the concept of SSF in ferromagnetic systems remains useful, although not in single films, as previously envisaged. Instead, we propose a trilayer structure. Exchange coupling between two FIs' magnetizations via a normal metal can secure an antiparallel configuration. We demonstrate that such synthetic antiferromagnets maintain long-range SSF over distances much greater than the exchange length. We also show that even when the two films differ, a spin supercurrent and, ultimately, a long-range non-SSF spin current can flow over sufficiently long distances in typical realizations.

The setup in Ref. [4] nicely illustrates SSF behavior. The spin Hall effect (SHE) leads to spin injection. In turn, spin-transfer torque (STT) causes the magnetization to precess, thereby leading to SP out of the opposite contact detected via the inverse SHE. This geometry therefore requires the contacts to be attached to the thin sides of the FI. The resulting resistance per area can be expressed in the form of an Ohm's law combining the interface resistances and an internal resistance,

$$r = 1/g_L^{\perp} + 1/g_R^{\perp} + r_\alpha, \tag{1}$$

where $g_L^{\perp}$ and $g_R^{\perp}$ are the transverse interface spin conductances, and the internal spin-relaxation-induced resistance is $r_\alpha = g_\alpha/(g_R^{\perp} g_L^{\perp})$, where $g_\alpha = 2e^2 M_s L \alpha_0/\hbar^2\gamma$. Here, M_s is the saturation magnetization, α_0 is the intrinsic Gilbert damping coefficient, γ is the gyromagnetic ratio, and L is the system length. The system exhibits SSF because the internal resistance r_α vanishes when $\alpha_0 \to 0$. With spin dissipation, the internal resistance increases algebraically with the length of the system.

To further utilize SSF, we suggest using a larger injection area with a spin valve attached to the top of the FI; see Fig. 1(a). Ignoring dipole interactions, Ohm's law [Eq. (1)] remains valid, but the intrinsic conductance becomes

$$g_\alpha = \frac{4\pi M_s \mathcal{V} \alpha_0}{\hbar\gamma \mathcal{A}_c} \frac{e^2}{h}, \tag{2}$$

where $\mathcal{V}$ is the FI volume and $\mathcal{A}_c$ is the injection or detection contact area. One can hence conclude that the SSF can be made arbitrarily long range by increasing the contact area in proportion to the system volume. Without dipole interactions, the SSF is limited only by the contact conductances, and a spin current can flow over macroscopic lengths. However, as discussed below, dipole interactions dramatically reduce the applicability of this finding.

In the geometry employed herein, a spin current is injected using the left contact (L), which consists of a spin valve with two ferromagnets, $F_{L,1/2}$, that exhibit perpendicular magnetic anisotropy and are coupled to a normal metal, N_L; see Fig. 1(a). Assuming an effective conductance across the $N_L|$FI interface, $\tilde{g}_{\mathrm{FI}}$, and low spin memory loss in N_L, we find that the injected spin accumulation in N_L, $\boldsymbol{\mu}_L = \mu_L \hat{z}$, is $\mu_L = eV_i(g_\uparrow - g_\downarrow)/(g_\uparrow + g_\downarrow + \tilde{g}_{\mathrm{FI}})$ [14]. Here, $g_{\uparrow(\downarrow)}$ is the conductance of the majority (minority) electrons across the two $F_{L,1/2}|N_L$ interfaces. This spin accumulation then drives the FI dynamics of the local magnetization direction, $\mathbf{m}(\mathbf{r}, t)$, at position $\mathbf{r}$ and time t. The spin angular momentum transported through the FI thin film is subsequently detected by the right contact (R), which consists of a normal metal, N_R, connected to a ferromagnet, F_R. The spin accumulation pumped into N_R is, in the limit of low spin-memory loss, $\boldsymbol{\mu}_R(\boldsymbol{r}) = -\hbar\mathbf{m} \times \dot{\mathbf{m}}|_{r\in \mathrm{R}}$ and can be measured according to the voltage, V_d, across the $N_R|F_R$ junction.

At low temperatures, SSF can be described semiclassically [3–6] and the magnetization dynamics are given by the Landau-Lifshitz-Gilbert (LLG) equation,

$$\dot{\mathbf{m}} = -\gamma \mathbf{m} \times \mathbf{H}_{\mathrm{eff}} + \alpha \mathbf{m} \times \dot{\mathbf{m}} - \alpha' \mathbf{m} \times \mathbf{m} \times \boldsymbol{\mu}/\hbar, \tag{3}$$

where, in the left (right) contact region, the spin accumulation $\boldsymbol{\mu} = \boldsymbol{\mu}_{L(R)}$ and $\alpha' = \alpha_{L(R)}$; both quantities are zero otherwise. The dimensionless parameter $\alpha_{L(R)} = g_{L(R)}^{\perp} \hbar^2\gamma/2e^2 M_s d$, where d is the FI thickness. The local

Gilbert damping coefficient is $\alpha = \alpha_0 + \alpha'$, where α' is the spin-pumping enhancement. The effective field, $\mathbf{H}_{\text{eff}}$, consists of the exchange field, $\mathbf{H}_{\text{ex}} = 2A/(M_s)\nabla^2\mathbf{m}$, where A is the exchange constant, and the dipole field, $\mathbf{H}_{\text{dip}}^{\text{tot}}$, which fulfills Maxwell's equations in the magnetostatic approximation,

$$\nabla \times \mathbf{H}_{\text{dip}}^{\text{tot}} = 0, \qquad \nabla \cdot (\mathbf{H}_{\text{dip}}^{\text{tot}} + 4\pi M_s \mathbf{m}) = 0. \tag{4}$$

The dipole field is related to the local magnetization by Green's functions: $\mathbf{H}_{\text{dip}}^{\text{tot}} = 4\pi M_s \int_{\mathcal{V}} d^3\mathbf{r}' \hat{G}(\mathbf{r} - \mathbf{r}')\mathbf{m}(\mathbf{r}', t)$, where $\hat{G}$ is a 2nd-rank tensor whose elements are $G_{\alpha\beta} = -(1/4\pi)\partial^2_{\alpha\beta'}(1/|\mathbf{r} - \mathbf{r}'|)$ [15]. We consider a FI thinner than the magnetic exchange length, $d \lesssim l_{\text{ex}} = \sqrt{A/2\pi M_s^2}$, such that any variation of $\mathbf{m}$ across the thickness is negligible. Then, one can divide the total dipole field into an easy plane term, $\mathbf{H}_{\text{EP}} = -4\pi M_s m_z \hat{z}$, and the remainder of the dipole field, $\mathbf{H}_{\text{dip}}$.

The dipole field $\mathbf{H}_{\text{dip}}$ causes the spin-wave eigenspectrum to depend strongly on the spin-wave propagation direction relative to the magnetization [11]. At long wavelengths and no applied magnetic field, spin waves propagating with wave vectors $k_{\parallel(\perp)}$ parallel (perpendicular) to the magnetization are exchange (dipole) dominated, and their frequency is $\omega(k_\parallel) = \gamma k_\parallel \sqrt{8\pi A}$ ($\omega(k_\perp) = 4\pi M_s \gamma \sqrt{2k_\perp d}$). Because SSF is associated with the steady-state solutions of Eq. (3) in which the magnetization performs 2π precessions, the relative orientation of the transport direction and the magnetization alternates between the exchange- and dipole-dominated regimes. Nonlocal dipole interactions are therefore critically important. However, the full inclusion of these interactions transforms the LLG equation [Eq. (3)] into a complicated second-order nonlinear integro-differential equation in time and in-plane coordinates, and thus, finding its solution requires considerable numerical efforts. For this purpose, we performed graphics processing unit (GPU)-accelerated micromagnetic simulations on several computers over a long time period [16].

We first consider a square YIG thin film. This geometry creates two dipole-induced easy axes that extend diagonally across the sample in addition to the easy plane anisotropy. The injection and detection contacts cover 20% of the thin film's surface area, as shown in Fig. 1(b). Hence, the ratio $\mathcal{A}_c/\mathcal{V} = 1/(5d)$ that controls the internal conductance [Eq. (2)] is independent of the length L. We further neglect any spin-memory loss inside the contacts because of the long spin-diffusion length of the Cu contacts, $l_{\text{sf}}^{\text{Cu}} =$ 100–1500 nm [17]. In line with typical transverse (mixing) conductance values [18,19] for Cu|YIG interfaces, we choose $g_{L/R}^{\perp} h/e^2 = 5 \times 10^{14}$ cm^{-2}, which, combined with $d_{\text{YIG}} = 5$ nm, yields $\alpha_{L/R} \approx 0.01$. We also use $4\pi M_s =$ 1750 G [11], $A = 3.7 \times 10^{-7}$ erg/cm [20], and $\alpha_0 = 1 \times 10^{-3}$ [18,19]. Typical values for the tunnel conductances for perpendicularly magnetized spin valves [21], $g_\uparrow h/e^2 \sim 10^{11}$ cm^{-2} and $g_\downarrow h/e^2 \sim 10^{10}$ cm^{-2}, give an applied voltage for the left contact of $V_i \sim 10$ mV, which corresponds to $\mu_L \sim 1$ μeV. This applied voltage produces a current density of 10^4 A cm^{-2}. The $N_R|F_R$ interface is similarly assumed to be a tunnel interface; therefore, the SP current across the FI$|N_R$ is compensated by the STT generated by $\boldsymbol{\mu}_R$. Generally, $\boldsymbol{\mu}_R$ contains both ac and dc components. We denote the z component of the dc spin accumulation in the right contact averaged over the contact area by $\langle \mu_R^z \rangle$ and investigate its behavior as a function of μ_L and the system size.

In the micromagnetic simulations, we start in a uniform state and let this state evolve into a steady state; see Fig. 2(a). Figures 2(b) and 2(c) show the steady-state spin accumulation $\langle \mu_R^z \rangle$ as a function of μ_L and L, respectively. A finite $\langle \mu_R^z \rangle$ can be observed only above a threshold μ_L^{thr} in panel (b). From Fig. 2(c) this threshold can be seen as a sudden drop of $\langle \mu_R^z \rangle$ as a function of L. The threshold is attributed to shape-induced pinning of the magnetization, and it can be seen to rapidly increase from $\mu_L^{\text{thr}} = 1$ μeV at $L \sim 300$ nm to $\mu_L^{\text{thr}} = 5$ μeV at $L \sim 350$ nm. When the threshold is overcome, $\langle \mu_z^R \rangle$ increases linearly with μ_L and is a constant function of L, as expected based on Eq. (2). Consequently, the transport in this region is identified as SSF. When the μ_L is increased further, $\langle \mu_z^R \rangle$ saturates. This saturation is caused by the interplay of the shape anisotropy and nonlocal magnon-magnon interactions. For large systems, this interaction is more efficient because of the reduced spin-wave energy separation. The saturation of $\langle \mu_R^z \rangle$ is analogous to the leveling off of the cone angle in a ferromagnetic resonance (FMR) experiment as a function of applied power because of magnon-magnon-interaction-mediated Suhl instabilities: when the cone angle of the FMR mode reaches a critical value, spin waves are excited

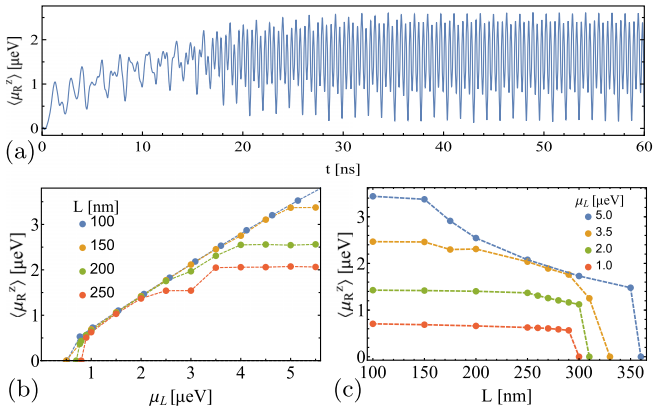

FIG. 2 (color online). (a) Time evolution of μ_R^z when $L = 250$ nm and $\mu_L = 3.0$ μeV. (b) The average dc spin accumulation in the right contact, $\langle \mu_R^z \rangle$, as a function of the spin accumulation in the left contact, μ_L, in samples with fixed lengths, L, and square geometries. (c) $\langle \mu_R^z \rangle$ as a function of L.

and power is lost from the FMR mode to the spin waves [22,23]. The onset of the $\langle\mu_z^R\rangle$ saturation is observed to occur at a lower value $\mu_L^{\rm sat}$ for increasing L, from $\mu_L^{\rm sat} \sim 5\ \mu$eV at $L = 150$ nm to $\mu_L^{\rm sat} \sim 3\ \mu$eV at $L = 250$ nm. Because $\mu_L^{\rm sat}$ decreases with increasing L, the interval in which SSF is possible, $\mu_L^{\rm thr} < \mu_L < \mu_L^{\rm sat}$, shrinks with increasing L until $\mu_L^{\rm sat} < \mu_L^{\rm thr}$. This "squeezing" effect restricts SSF to samples for which $L < 300$ nm.

Next, we analyze FI thin films with circular geometries, see Fig. 1(c). Such high-symmetry structures are chosen because the absence of an easy axis leads to much longer spin-current propagation lengths. Figures 3(a) and 3(b) show $\langle\mu_R^z\rangle$ as a function of μ_L and diameter D, respectively. The squeezing effect described above is observed but now with $\mu_L^{\rm thr} = 0$. At $D = 500$ nm, $\langle\mu_R^z\rangle$ follows the SSF result only for $\mu_L \leq 1\ \mu$eV. For larger μ_L or D, spin transport persists, even for micron sized disks, but is less efficient (and shows larger resistance) than SSF [Eq. (2)].

Finally, we demonstrate that long-range SSF can be recovered in a synthetic antiferromagnet structure. When two FI thin films are in contact via a thin normal metal, RKKY interaction can lead to antiferromagnetic exchange coupling between the two layers [24]. In the absence of an external magnetic field, the ground state has an antiparallel configuration with zero net magnetization. Dipolar interactions are then suppressed over distances longer than the trilayer thickness and only the easy-plane anisotropy term survives in the thin-film limit.

By applying spin accumulation to the top FI in the same manner as for the single-layer FI, one can induce a rotation of the FIs' magnetizations that maintains the net magnetization near zero. Under steady-state conditions, the SP current that flows from FI1 into the spacer layer is exactly compensated by the SP current that flows from FI2, thereby resulting in a vanishing SP + STT torque, and vice versa. Hence, the RKKY interaction dominates the interlayer interaction. Writing the magnetizations as $\mathbf{m}_{1/2}(\mathbf{r},t) = (\pm[1-m_{1/2,z}^2]^{1/2}\cos\phi_{1/2}, \pm[1-m_{1/2,z}^2]^{1/2}\sin\phi_{1/2}, m_{1/2,z})$, and assuming that $(m_{1,2})_z \ll 1$ and $|\phi_1 - \phi_2| \ll 1$, the SSF hydrodynamic equations for the first layer are

$$\dot{m}_{1,z} = \frac{2\gamma A}{M_{s,1}}\nabla^2\phi_1 - \alpha_1\dot{\phi}_1,$$
$$\dot{\phi}_1 = [4\pi M_{s,1}\gamma + \omega_{E,1}]m_{1,z} + \omega_{E,1}m_{2,z} + \alpha_1\dot{m}_{1,z}. \quad (5)$$

(For layer 2, interchange 1↔2.) Here, $M_{s,1(2)}$ is the saturation magnetization of layer 1(2) and $\alpha_1 = \alpha_{0,1} + \alpha_1'$, where $\alpha_{0,1}$ is the intrinsic Gilbert damping in FI1 and $\alpha_1' = \alpha_{L(R)}$ under the left (right) contact area and zero otherwise. FI2 is not attached to any external contacts, i.e., $\alpha_2' = 0$, and the damping is dominated by the layer's intrinsic Gilbert damping, $\alpha_2 = \alpha_{0,2}$. The strength of the RKKY interaction is parameterized by $\omega_{E,1(2)}$ [25]. The left and right contacts are attached to layer 1 and provide additional STT and SP, as in the single-layer cases.

For small values of $\boldsymbol{\mu}_L$, the spatial variation of $\mathbf{m}_{1/2}$ is small. Assuming symmetric layers, i.e., $M_{s,1} = M_{s,2} = M_s$, $\alpha_{0,1} = \alpha_{0,2} = \alpha_0$, and $\omega_{E,1} = \omega_{E,2} = \omega_E$, we obtain

$$\langle\mu_R^z\rangle = -\hbar\Omega = \frac{g_L^\perp}{g_L^\perp + g_R^\perp + g_\alpha}\mu_L, \quad (6)$$

$m_z = -\Omega/(2\omega_E + 4\pi M_s\gamma)$, and $(\phi_1 - \phi_2) \sim \alpha_2\Omega/\omega_E$, where g_α is the intrinsic conductance defined in Eq. (2) with the substitution $\alpha_0 \to \alpha_{0,1} + \alpha_{0,2}$. Equation (6) can be identified as Ohm's law, Eq. (1).

Figure 3(c) shows the exact numerical result for $\langle\mu_R^z\rangle$ as a function of μ_L for a trilayer structure composed of two disks, each with a thickness of $d_{\rm YIG} = 5$ nm and a coupling $\omega_E = 7.3 \times 10^{10}\ {\rm s}^{-1}$, where the dipole interaction is fully included. The detector signal is close to the ideal value given by Eq. (6), even for micrometer-sized systems. Saturation also occurs in trilayer systems but at much higher values of μ_L than for single-layer films; despite the relatively large variations in ϕ, SSF remains stable because of screening of the dipole interactions. Figure 3(d) shows that spin transport is possible over much greater distances in trilayer structures than in single-layer ones: the single-layer $\langle\mu_R^z\rangle$ exhibits a 75% spin-signal reduction over the D interval 0.1–2.0 μm, whereas the trilayer only exhibits a 25% reduction over the same interval and a 50% reduction at $D = 4\ \mu$m. The SSF is robust against small variations in the FI layer properties; see Fig. 3(d). Our results demonstrate that trilayer structures are able to support SSF currents for system sizes up to ~1 μm and long-range spin transport across samples that are several micrometers in size.

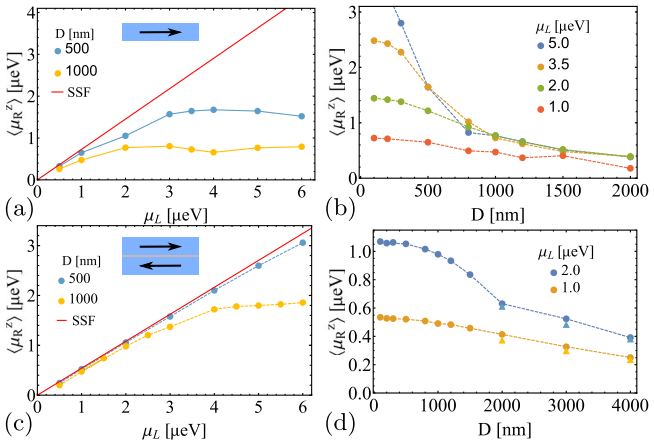

FIG. 3 (color online). The average dc spin accumulation in the right contact, $\langle\mu_R^z\rangle$, as a function of (a) μ_L and (b) D for a disk-shaped thin film. $\langle\mu_R^z\rangle$ as a function of (c) μ_L and (d) D for disk-shaped trilayer samples for symmetric trilayer structures with $M_{s,1/2} = M_s$ (circles) and asymmetric layers with $M_{s,1/2} = (1 \pm 0.1)M_s$ (triangles). The solid red lines in (a) and (c) represent the theoretical SSF values of $\langle\mu_R^z\rangle$.

In summary, we have investigated SSF in FI thin films. The dipole field qualitatively alters the transport properties so that single-layer SSF is possible only in systems that are less than a few hundred nanometers in size. Suppression of the dipole field in trilayer structures enables long-range spin transport mediated by SSF over length scales up to $\sim 1\ \mu$m and by non-SSF magnetization dynamics over length scales up to several micrometers.

We gratefully acknowledge useful discussions with Peder Notto Galteland. This work was supported by EU FP7 FET Grant No. 612759.

*hans.skarsvag@ntnu.no

[1] J. König, M. Chr. Bønsager, and A. H. MacDonald, Phys. Rev. Lett. **87**, 187202 (2001).
[2] F. S. Nogueira and K.-H. Bennemann, Europhys. Lett. **67**, 620 (2004).
[3] E. B. Sonin, Adv. Phys. **59**, 181 (2010).
[4] S. Takei and Y. Tserkovnyak, Phys. Rev. Lett. **112**, 227201 (2014).
[5] H. Chen, A. D. Kent, A. H. MacDonald, and I. Sodemann, Phys. Rev. B **90**, 220401 (2014).
[6] S. Takei and Y. Tserkovnyak, Phys. Rev. Lett. **115**, 156604 (2015).
[7] K. Nakata, K. A. van Hoogdalem, P. Simon, and D. Loss, Phys. Rev. B **90**, 144419 (2014).
[8] P. Clausen, D. A. Bozhko, V. I. Vasyuscka, G. A. Melkov, B. Hillebrands, and A. A. Serga, arXiv:1503.00482.
[9] P. Pirro, T. Brächer, A. V. Chumak, B. Lägel, C. Dubs, O. Surzhenko, P. Görnert, B. Leven, and B. Hillebrands, Appl. Phys. Lett. **104**, 012402 (2014).
[10] B. A. Kalinikos and A. N. Slavin, J. Phys. C **19**, 7013 (1986).
[11] A. A. Serga, A. V. Chumak, and B. Hillebrands, J. Phys. D **43**, 264002 (2010).
[12] S. O. Demokritov, V. E. Demidov, O. Dzyapko, G. A. Melkov, A. A. Serga, B. Hillebrands, and A. N. Slavin, Nature (London) **443**, 430 (2006).
[13] A. V. Chumak, A. A. Serga, and B. Hillebrands, Nat. Commun. **5**, 4700 (2014).
[14] A. Brataas, Y. V. Nazarov, and G. E. W. Bauer, Phys. Rev. Lett. **84**, 2481 (2000).
[15] A. G. Gurevich and G. A. Melkov, *Magnetic Oscillations and Waves* (CRC, New York, 1996).
[16] A. Vansteenkiste, J. Leliaert, M. Dvornik, M. Helsen, F. Garcia-Sanchez, and B. Van Waeyenberge, AIP Adv. **4**, 107133 (2014).
[17] E. Villamor, M. Isasa, L. E. Hueso, and F. Casanova, Phys. Rev. B **88**, 184411 (2013).
[18] H. L. Wang, C. H. Du, Y. Pu, R. Adur, P. C. Hammel, and F. Y. Yang, Phys. Rev. Lett. **112**, 197201 (2014).
[19] C. Du, H. Wang, F. Yang, and P. C. Hammel, Phys. Rev. Applied **1**, 044004 (2014).
[20] S. Klingler, A. V. Chumak, T. Mewes, B. Khodadadi, C. Mewes, C. Dubs, O. Surzhenko, B. Hillebrands, and A. Conca, J. Phys. D **48**, 015001 (2015).
[21] S. Ikeda, K. Miura, H. Yamamoto, K. Mizunuma, H. D. Gan, M. Endo, S. Kanai, J. Hayakawa, F. Matsukura, and H. Ohno, Nat. Mater. **9**, 721 (2010).
[22] H. Suhl, Phys. Chem. Solids **1**, 209 (1957).
[23] N. Bahlmann, R. Gerhardt, M. Wallenhorst, and H. Dötsch, J. Appl. Phys. **80**, 3977 (1996).
[24] S. S. P. Parkin, Phys. Rev. Lett. **67**, 3598 (1991).
[25] P. Grünberg, R. Schreiber, Y. Pang, M. B. Brodsky, and H. Sowers, Phys. Rev. Lett. **57**, 2442 (1986).